Analyst

PAPER

View Article Online
View Journal | View Issue

Cite this: *Analyst*, 2014, **139**, 4681

Preparation of biofunctionalized quantum dots using microfluidic chips for bioimaging†

Siyi Hu,‡[abd] Shuwen Zeng,‡[bc] Butian Zhang,[b] Chengbin Yang,[b] Peiyi Song,[b] Tng Jian Hang Danny,[b] Guimiao Lin,[e] Yucheng Wang,[b] Tommy Anderson,[b] Philippe Coquet,[c] Liwei Liu,*[ad] Xihe Zhang[ad] and Ken-Tye Yong*[b]

Biofunctionalized quantum dots (QDs), especially protein-coated QDs, are known to be useful targeted fluorescent labels for cellular and deep-tissue imaging. These nanoparticles can also serve as efficient energy donors in fluorescence resonance energy transfer (FRET) binding assays for the multiplexed sensing of tumor markers. However, current preparation processes for protein-functionalized QDs are laborious and require multiple synthesis steps (*e.g.* preparing them in high temperature, making them dispersible in water, and functionalizing them with surface ligands) to obtain a high quality and quantity of QD formulations, significantly impeding the progress of employing QDs for clinical diagnostics use such as a QD-based immunohistofluorescence assay. Herein, we demonstrate a one-step synthesis approach for preparing protein-functionalized QDs using a microfluidic (MF) chip setup. Using bovine serum albumin (BSA) molecules as the surface ligand model, we first studied and optimized the MF reaction synthesis parameters (*e.g.* reaction temperature, and channel width and length) for making protein-functionalized QDs using COMSOL simulation modeling, followed by experimental verification. Moreover, in comparison with the BSA-functionalized QDs synthesized using the conventional bench-top method, BSA–QDs prepared using the MF approach exhibit a significantly higher protein-functionalization efficiency, photostability and colloidal stability. The proposed one-step MF synthesis approach provides a rapid, cost effective, and a small-scale production of nanocrystals platform for developing new QD formulations in applications ranging from cell labeling to biomolecular sensing. Most importantly, this approach will considerably reduce the amount of chemical waste generated during the trial-and-error stage of developing and perfecting the desired physical and optical properties of new QD materials.

Received 30th April 2014
Accepted 27th June 2014

DOI: 10.1039/c4an00773e

www.rsc.org/analyst

1. Introduction

Microfluidic chips are a promising platform for lab-on-a-chip applications such as single cell analysis, chemical sensing, and contaminant monitoring in water.[1–6] With the dimensions of the flow channels in the scale of hundreds of micrometers, small amounts of sample fluids (*e.g.*, nanoliter to picoliter volumes) can be processed or manipulated within the MF chip.[7] Compared to the conventional hot colloidal synthesis method, using a microfluidic chip to prepare the desired QDs provides several unique advantages: (i) only a small amount of materials and reagents are required for preparing QDs, which avoids generating large volumes of chemical wastes; (ii) using a microfluidic chip allows the fabrication of QDs within minutes, which enables the rapid testing of a series of QD recipes by employing multiple MF chips; (iii) the reaction temperature, reagent mixing, and reaction time for the synthesis of QDs can be precisely controlled, which generates a significantly narrower particle-size distribution;[8] (iv) low thermal mass and large surface to volume ratio of the MF channels allow rapid heat transfer to the desired reaction region, which helps to promote the homogeneous nucleation of QD seeds, which helps in producing QDs fluorescence spectrum with the desired emission peaks;[8] and (v) the microfluidic devices can be modified and integrated with additional parts for preparing multifunctional and multimodal QDs for *in vivo* imaging[9,10] and drug delivery therapy applications.[11,12] The first nanoparticle

[a]*School of Science, Changchun University of Science and Technology, Changchun 130022, Jilin, China. E-mail: liulw@cust.edu.cn*

[b]*School of Electrical and Electronic Engineering, Nanyang Technological University, Singapore 639798, Singapore. E-mail: ktyong@ntu.edu.sg*

[c]*CINTRA CNRS/NTU/THALES, UMI 3288, Research Techno Plaza, 50 Nanyang Drive, Border X Block, Singapore 637553, Singapore*

[d]*International Joint Research Center for Nanophotonics and Biophotonics, Changchun University of Science and Technology, Changchun 130022, Jilin, China*

[e]*The Engineering Lab of Synthetic Biology and the Key Lab of Biomedical Engineering, School of Medicine, Shenzhen University, Shenzhen 518060, China*

† Electronic supplementary information (ESI) available. See DOI: 10.1039/c4an00773e

‡ These authors contributed equally to this work.

synthesis using microfluidic chip was reported by Mello and co-workers in 2002.[13] They demonstrated that the polydispersity of CdS nanoparticles was significantly reduced by a continuous flow-based microfluidic chip setup. Since then, various metallic, metal oxide, magnetic and semiconductor nanoparticles, such as Ag,[14,15] Au,[16,17] Co,[18,19] TiO_2,[20–22] Fe_3O_4,[23] SiO_2,[24] CdSe,[25–27] CdTe,[8] ZnSe,[28] PbS,[8] InP,[29] and even more complicated core/shell nanostructures, such as CdSe/ZnS,[30] Fe_2O_3/SiO_2,[31] ZnSe/ZnS,[32] and ZnS/CdSe/ZnS,[33] have been successfully prepared using microfluidic devices.[34] It is worth noting that the reproducibility of preparing nanoparticles with identical physical and chemical properties can be achieved by a microfluidic chip and this is beneficial for producing high quality QD-based assays (*e.g.* immunofluorescence assays) for applications in clinical diagnosis.[35]

Among the abovementioned nanoparticles, colloidal QDs have attracted significant attention from biomedical and life science research communities because of their effectiveness in bioimaging and drug screening applications.[36–38] For instance, the emission peak of CdTe QDs can be tuned from the visible region to near-infrared (NIR) wavelength region by changing their particle size,[39] and such a unique feature allows their use for the multicolor fluorescence imaging of cells.[40] Carbon nanodots (CQDs) and graphene quantum dots (GQDs) are another class of promising nanoparticles for bioimaging and nanomedicine application. We expect that such nanoparticles may be more acceptable for clinical studies because they are made from benign carbon material.[41–45] To apply QDs for imaging and sensing applications, such as optical immunosensing and *in vivo* tumor imaging, the QDs require to be functionalized with targeting ligands (*e.g.*, protein, DNA, RNA, peptides, and lipids) for the targeted labeling of desired cells and biomarkers.[46] To date, the direct synthesis of biofunctionalized QDs still remains a challenge. Very little success has been achieved using the conventional bench-top synthesis method to produce biofunctionalized QDs in a single step. This is mainly because of the following reasons: (i) high temperature (higher than 100 °C) and long reaction time (more than 10 hours) are required to produce high crystalline QDs, and such harsh process conditions generally degrade the biomolecules; (ii) if the synthesis of the QDs is carried out under mild conditions, the photoluminescence intensity and optical and colloidal stability of the biofunctionalized QDs will be significantly compromised. Currently, the preparation of biofunctionalized QDs requires complex and tedious processing steps such as the solubilization of QDs in water, functionalization of biomolecules, and purification of QDs.[47,48] Thus, there is a requirement to engineer new approaches to rapidly synthesize biofunctionalized QDs in a single step method, thereby allowing greater use of these QDs in biological applications without the requirement of other processing steps.

In this study, we report the use of a microfluidic chip for the one-step synthesis of BSA-functionalized CdTe QDs. This approach addresses the main challenges faced by the conventional synthesis method. Prior to fabricating the microfluidic chip for the synthesis of QDs, we first employed the COMSOL multiphysics finite element simulation technique to design and optimize the microfluidic reaction channel parameters (*e.g.*, reaction temperature, and channel width and length) for preparing QDs in a laminar flow model. Once our device design was optimized, these parameters were used as references to fabricate microfluidic chips for making QDs in aqueous phase. The prepared BSA–QDs from the microfluidic chip device (MF) were then characterized by UV-Vis absorbance (Abs) and photoluminescence (PL) spectroscopy, Fourier transform infrared spectroscopy (FT-IR) and agarose gel electrophoresis. Compared to the BSA–QDs that were obtained from the conventional bench-top colloidal synthesis method (BT), the BSA–QDs synthesized by the microfluidic device displayed a higher degree of functionalization of BSA and a significant improvement in the optical and colloidal stability of the QDs. In addition, we demonstrated that this MF method can be extended to preparing QDs functionalized with folic acids and these bioconjugates can be used for the targeted imaging of cancer cells.

2. Results and discussion

In our one-step synthesis of CdTe QDs using the MF approach, 3-mercaptopropionic acid (MPA) and BSA molecules were used as surface ligands to stabilize and control the growth of QDs in an aqueous dispersion. Basically, BSA molecules bind to the surface of the QDs through the coordination of amino acid residues with Cd^{2+} ions, while MPA molecules passivate the surface for enhancing the colloidal stability of the nanocrystals. In this work, we first investigate the effects of reaction temperature on the growth rate of QDs in the microfluidic chip. Using the reaction engineering (re) model in COMSOL Multiphysics 4.3a, the relationship between the concentration of the synthesized QD and residence time (*i.e.*, the reaction time of QDs inside the microfluidic channel) can be theoretically predicted. The initial concentrations of Cd^{2+} and Te^{2-} solutions injected into the inlets of microfluidic chip were set at 10 mM and 3.3 mM, which provided a Cd/Te concentration ratio of 1 : 0.3. This ratio was fixed in all of our experimental and simulation studies. When the reaction temperature increased from 50 °C to 100 °C, the concentration of the QDs increased from 1.6 mM to 2.4 mM after 5 min reaction time (see Fig. 1a), which indicated that increasing the reaction temperature promotes faster growth rate of QDs. The distribution profiles of the concentrations of BSA–QDs synthesized in the microfluidic reaction channel of 200 μm height and 200 μm width at various reaction temperatures (50, 65, 85 and 100 °C) are plotted in Fig. 2. We then carried out the actual synthesis of QDs using the MF approach under the same reaction temperatures for verification with the simulation data. In Fig. 1b, one can clearly see that the total number of synthesized BSA–QDs particles increases as the reaction temperature increases. The number of generated QDs increases from 1.90×10^{18} L^{-1} to 3.19×10^{18} L^{-1} when temperature increases from 50 °C to 100 °C. The obtained experimental result agrees well with the simulation data. In our case, the number of QD particles was estimated by using Beer–Lambert's law,[49] and we assumed the size of CdTe to be 1.5 nm in the estimation because the emission peaks of the

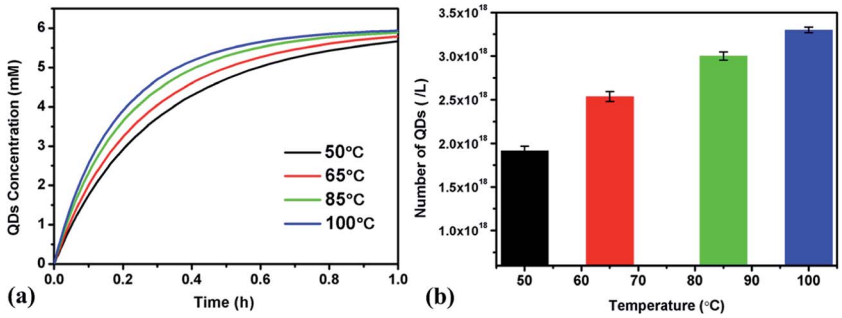

Fig. 1 Simulation results (a) and experimental measurements (b) of BSA–QDs synthesized *via* the MF method under different reaction temperatures (50, 65, 85 and 100 °C). All the experiments in (b) were carried out at the same reaction time of 5 min.

prepared QD products are mostly centered at 460 nm. To further understand the effects of reaction temperature on the growth kinetics of QDs, a one-step MF synthesis of MPA-attached CdTe QDs is also demonstrated. In this experiment, BSA molecules were not utilized because the reaction temperatures employed here are greater than 100 °C, which would denature protein molecules. Thus, we used MPA molecules instead because they can withstand higher reaction temperatures. The simulation result is shown in Fig. 3a, and this shows that the concentration of MPA–CdTe QD products increased from 2.4 mM to 4.5 mM after 5 min of reaction time with reaction temperature increasing from 98 °C to 220 °C. Similarly, a same trend was observed in the experimental result when we prepared CdTe QDs at reaction temperatures ranging from 98 °C to 220 °C, as shown in Fig. 3b. The total number of MPA–CdTe QDs particles was estimated to increase from 3.18×10^{18} to 4.37×10^{18} L^{-1} when a higher temperature was applied during synthesis. For directly preparing a QDs aqueous dispersion in a three-necked flask, the maximum reaction temperature that can be applied is around 100 °C and any further increase in temperature will result in the vaporization of reaction medium and the disruption of colloidal and optical stability of the QDs.[40,50] Such challenges can be easily overcome by using the MF synthesis method. Because the reaction mixture is enclosed in a small space, MF reaction temperature for the aqueous phase QDs synthesis can be increased above 100 °C without the risk of the evaporation of reaction solution during fabrication. Actually, we demonstrate that MPA–CdTe QDs can be synthesized at temperature as high as 200 °C and in general this still produces high crystalline QDs with better quantum yields. More importantly, this will significantly reduce the reaction time required for producing per batch QDs because a rapid heat transfer can

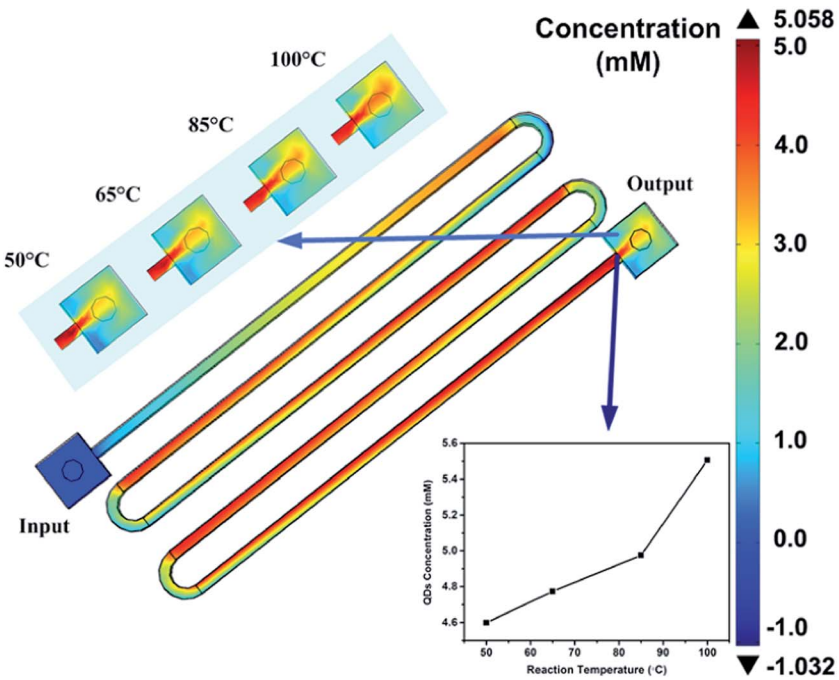

Fig. 2 Simulation prediction of the concentration distribution of BSA–QDs synthesized in microfluidic channel with a width of 200 μm under different reaction temperatures (50, 65, 85 and 100 °C).

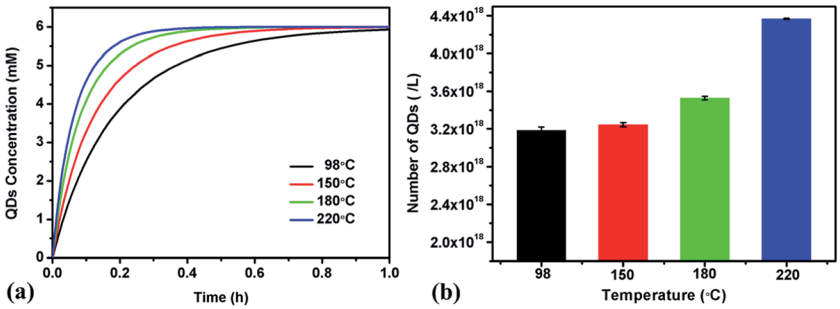

Fig. 3 Simulation results (a) and experimental measurements (b) of MPA–CdTe QDs in the aqueous phase synthesized *via* the MF method under different reaction temperatures (98, 150, 180 and 220 °C). All the experiments in (b) were carried out at the same reaction time of 5 min.

be achieved in a short burst by a high surface to volume ratio (SA : V) (~5000 m^{-1}) of the reaction channels (see eqn (1)) and low thermal mass of the reagents travelling within the channel system.[51]

$$\frac{WL}{WLH} = \frac{1}{H} \quad (1)$$

In eqn (1), W refers to the width of the channel, L is the channel length and H is the channel height. Based on the above-mentioned results, we can prepare multiple batches of QDs with different functionalities within 30 minutes by using the MF method, which significantly improves the procedures for optimizing the intended QDs formulations for specific biological applications.

To confirm the attachment of BSA molecules on the surface of QDs, agarose gel electrophoreses experiments were performed for the as-prepared QDs sample. From Fig. 4, one can see that the MPA-coated CdTe QDs exhibited a single band (upper band) with high mobility, while BSA-conjugated QDs exhibited another band (lower band) with retarded mobility because of their relatively large size when compared to that of the MPA–QDs. We observed that the luminescence intensity of BSA–QDs synthesized at 65 °C (lower band) is significantly stronger than that of the ones synthesized at 85 °C and 100 °C. Moreover, no luminescence intensity is observed from the upper band of the BSA–QDs prepared at 65 °C, indicating that most of the QDs are passivated with BSA molecules. The obtained gel electrophoresis result suggested that BSA molecules were mostly denatured under high reaction temperatures at 85 °C and 100 °C. In addition to agarose gel electrophoreses, the surface compositions of BSA–QDs synthesized at 65 °C were characterized by a FTIR spectrometer (see Fig. 5). The broad peaks of free BSA at 3448 cm^{-1}, BSA–Cd^{2+} ion at 3442 cm^{-1} and MF–BSA–QD at 3445 cm^{-1} are attributed to the O–H stretch of the BSA phenol group.[52] The blue shift of this broad peak from 3448 cm^{-1} indicated that the BSA phenol group of the tyrosine residue interacted with Cd^{2+} and CdTe QDs. The peaks of free BSA at 1653 cm^{-1} and 1454 cm^{-1} are attributed to the C=O stretch of the carboxyl group from glutamine and the C–N stretch of the imidazole group from the histidine residue, respectively. The intensities of these two peaks were significantly attenuated in the spectra of BSA–Cd^{2+} ion and MF–BSA–QD complex, indicating respective reaction of the carboxyl group and histidine residue with Cd^{2+} and CdTe QDs. The new peak of BSA–Cd^{2+} at 1107 cm^{-1} might be contributed to the interaction between Cd^{2+} and BSA. The peaks of BSA–(MPA) Cd^{2+} and MF BSA–(MPA) CdTe at 1402 cm^{-1} were attributed to the COO^- of MPA, which corresponded to the reaction of MPA with Cd^{2+} and CdTe QDs. FTIR result suggested that BSA molecules initially chelated with Cd^{2+} ions and remained bound to the surface of CdTe QDs[53,54] throughout the microfluidic synthesis process. Based on the abovementioned studies, we chose 65 °C as the optimum reaction temperature for preparing BSA-functionalized QDs using a microfluidic chip for biological applications.

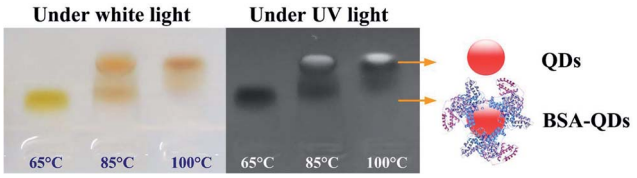

Fig. 4 Agarose gel electrophoresis of BSA–QDs synthesized *via* the MF method in 5 min under different reaction temperatures (65, 85 and 100 °C).

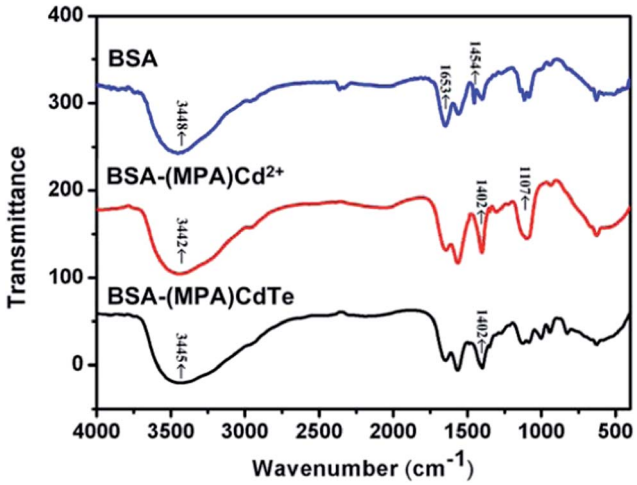

Fig. 5 FTIR spectra of free BSA, BSA–Cd^{2+} ion complex and MF–BSA–QD synthesized under 65 °C.

In addition to reaction temperature, the parameters (*e.g.*, width and length) of microfluidic channels play an important role in determining the final shape and size of the prepared nanoparticles.[1,7] Here, we first employed the transport of diluted species (*chds*) and laminar flow (*spf*) models in COMSOL Multiphysics 4.3a to provide a theoretical prediction of the generated QDs concentration and their corresponding velocity profiles within the MF channels. The channel height and the volumetric flow rate (*i.e.*, the pumping rate of the syringe containing reagents) in all the theoretical and experimental studies were fixed at 200 μm and 500 μL min^{-1}. The first parameter we investigated was the channel width of the MF system. Fig. 6a shows the predicted velocity profiles of the generated QDs in the MF channels with channel widths of 200 μm, 400 μm, and 600 μm, respectively. To save computation time and storage space, channel length was fixed at 50 mm. The flow velocity of the QDs concentration was estimated to reach the maximum state when an MF with a channel width of 200 μm was used. This can be explained by eqn (2), where flow velocity inside the MF channel is inversely proportional to channel width when the channel height and volumetric flow rate are fixed.[51]

$$v = \frac{Q}{A} = \frac{Q}{WH} \quad (2)$$

Here, v is the flow velocity, Q is the volumetric flow rate, A is the cross-sectional area of the microfluidic channel, W is the width of the channel and H is the channel height. To confirm and test the accuracy level of our calculation, we carried out one-step syntheses of the BSA–QDs formulation using microfluidic chips with channel widths of 200 μm, 400 μm and 600 μm and a fixed channel length of 800 mm. The reactions were carried out at the optimum reaction temperature of 65 °C. As shown in Fig. 6b, the number of BSA–QD particles increases with decreasing channel width from 600 μm to 200 μm and the number of BSA–QDs particles increased from 1.59×10^{18} L^{-1} to 2.82×10^{18} L^{-1}. This result is attributed to higher flow velocity inside the MF channel at 200 μm, which effectively prevents the deposition of QD by-products on the channel wall. In addition, the narrower MF channel width generally results in a more homogeneous reaction, and thus producing BSA–QDs particles with higher monodispersity sizes.[25,34] The second MF parameter we investigated was the MF channel length. The simulation result in the top left inset of Fig. 6a indicates that the concentration of the BSA–QD particles increases from 5.058 mM to 6.954 mM when 2.5 times longer channel length was used. The experimental result in Fig. 6b also shows that the number of BSA–QD particles increases when the total channel length increased from 800 mm to 2000 mm. Based on these results, we conclude that longer MF channel length generally delays the continuous residence time for the reaction of QDs (*i.e.*, the reaction time of QDs inside the microfluidic channel), and thus creates a larger population of QDs within the channel.[27,34] The generated number of BSA–QDs particles using a 2000 mm length channel is estimated to be 2.96×10^{18} L^{-1}, which is considerably higher than that of the number of particles produced in 800 mm length channel. From Fig. 7, one can see that the PL intensity of the prepared BSA–QDs with a MF channel width and length of 200 μm and 2000 mm is significantly stronger than that of BSA–QDs synthesized using the conventional bench-top flask method for 4 hours, indicating that a higher growth kinetic rate of BSA–QDs can be

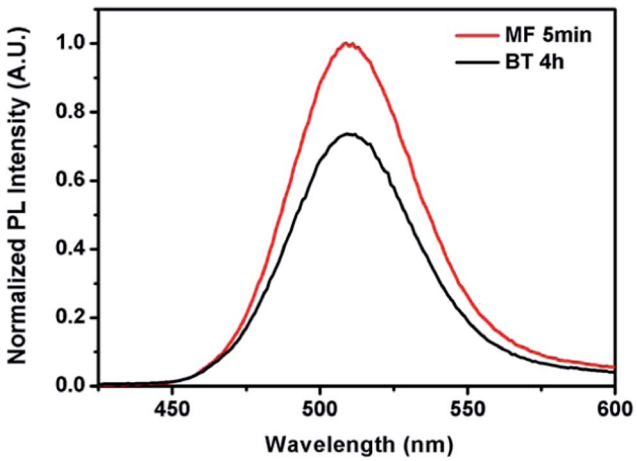

Fig. 7 Photoluminescence spectra of MF–BSA–QDs synthesized in 5 min (red line), BT–BSA–QDs synthesized in 4 hours (black line).

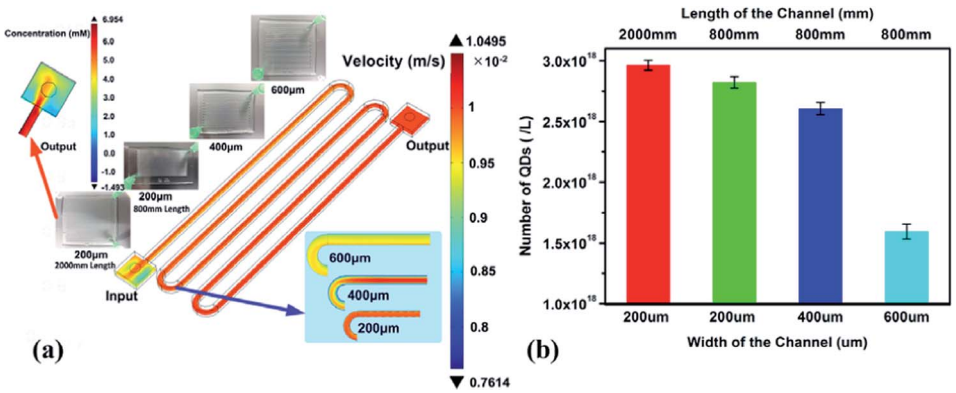

Fig. 6 Simulation results (a) and experimental measurements (b) of BSA–QDs synthesized *via* the MF method with different channel widths (200 μm, 400 μm and 600 μm) or lengths (800 mm and 2000 mm) under the optimum reaction temperature of 65 °C. All the experiments in (b) were carried out with the same reaction time of 5 min and a fixed volumetric flow rate of 500 μL min^{-1}.

achieved using the MF approach. The functionalization efficiency of BSA–QDs produced by the MF and BT approaches was also investigated by performing agarose gel electrophoresis testing. Fig. 8 shows the agarose gel electrophoresis data for produced BSA–QDs using either the MF or BT method. Using the same BSA concentration of 0.5 mg mL^{-1} in the MF and BT synthesis processes, the luminescence intensity from the lower band of BSA–QDs produced by the MF method is significantly stronger than that of the BSA–QDs generated using the BT synthesis method. On the other hand, luminescence intensity from the upper band of QDs prepared with the MF technique is considerably weaker than that of the QDs prepared using the BT approach. The line of BSA concentration of 2.0 mg mL^{-1} shows that there are no QDs in the upper band and the BSA–QDs are all located at the lower band, suggesting that the QDs are conjugated with BSA at a BSA concentration of 2.0 mg mL^{-1}. This comparison clearly demonstrates that a higher functionalization efficiency of BSA molecules on the surface of QDs is achieved by the MF method compared with the BT technique, and the optimum concentration of BSA to conjugate with the QDs is 2.0 mg mL^{-1}.

The photostability and colloidal stability of QDs are important factors to be considered when utilizing them as optical probes for biological applications such as bioimaging.[55] Fig. 9 shows the PL maximum changes of BSA–QDs produced by the MF and BT methods but with the samples exposed to continuous UV radiation for different time periods. The PL signals of the QDs were carefully monitored and measured (Fig. S1†). In our experiment, a lower photobleaching rate was observed for BSA–QDs formulation prepared using the MF method when we increased the exposure time of UV radiation to the samples. More specifically, PL intensity drops by 74% after 7 hours of exposure to UV radiation in the case of the QDs produced by the MF approach. However, a drop of 90% is observed in the case of the QDs generated by the BT method. This clearly shows that the MF method produced QDs with better photostability compared with the BT technique. In addition to photostability experiments, we also performed QDs colloidal stability study. The colloidal stability of the prepared BSA–QDs was evaluated at pH values ranging from 5 to 12 for 60 hours. Their hydrodynamic sizes were monitored by dynamic light scattering (DLS) technique at room temperature, as shown in Fig. 10 and S2.† The BSA–QDs prepared by the MF and BT methods are relatively stable at a pH of 12. This may be because of rich hydroxide ions available at high pH values that facilitate the dissociation of

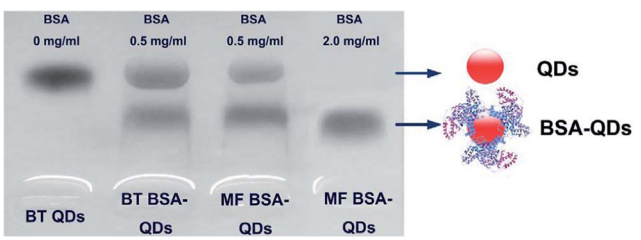

Fig. 8 Agarose gel electrophoresis of BT–MPA–QDs, BT–BSA–QDs and MF–BSA–QDs synthesized in 5 min under 65 °C.

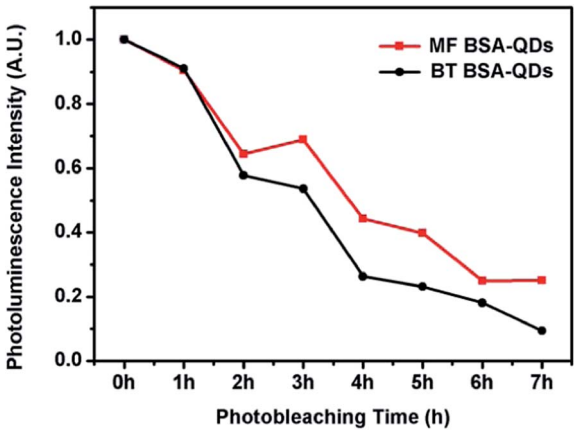

Fig. 9 Comparison of photostability between MF–BSA–QDs synthesized in 5 min and BT–BSA–QDs synthesized in 4 hours. The PL maximum changes for QDs at different UV irradiation time.

unbound anionic groups (*e.g.*, carboxyl groups) on BSA ligands and thus increase the surface charge density of QDs.[56] The formulation of BSA–QDs synthesized using the MF approach is considerably more stable in pH 5, 7 and 9 solutions when compared to those generated by the BT method. It is worth noting that BSA–QDs prepared by the BT method were more easily aggregated and precipitated from water compared to those generated by the MF approach. Overall, the colloidal stability of the BSA–QDs generally depends on the pH of the solution. Nevertheless, our results indicate that the MF method produces BSA–QDs formulations with considerably better colloidal stability.

For the bioimaging study, we employed the prepared BSA–QDs for labeling live cells. RAW264.7 macrophages cell were used in this experiment. As illustrated in Fig. 11a, a strong cellular uptake was observed for our MF–BSA–QDs formulation with a quantum yield (QY) of 16.23%. Green emission signals originated from the prepared QDs. This result indicates that the BSA–QDs prepared by the MF approach are suitable for use as an optical contrast agent for the imaging of cells and live animals. Using the same synthesis method, folic acids (FA)-functionalized CdTe QDs were also prepared in this study. FA is a commonly used cancer-homing agent for targeted drug delivery because its corresponding receptors (folate receptors) are known to be overexpressed in a variety of cancer cells. Fig. 11c shows the fluorescence images of Panc-1 cells stained with FA–QD bioconjugates. From the fluorescence images, FA-mediated targeting can be observed by the luminescent signal from the labeled cells, and the QDs were located in the vesicles within the cells. On the other hand, a weak QD signal was detected from the cancer cells treated with MPA–QDs in Fig. 11b, indicating that the uptake of QD bioconjugates occurred through specific interaction rather than by a passive uptake mechanism. In the near future, we expect that one could prepare a peptide- or antibody-conjugated QDs formulation using the MF method and that this could be conveniently used for the *in vivo* imaging of tumor vasculatures and tumor matrices.

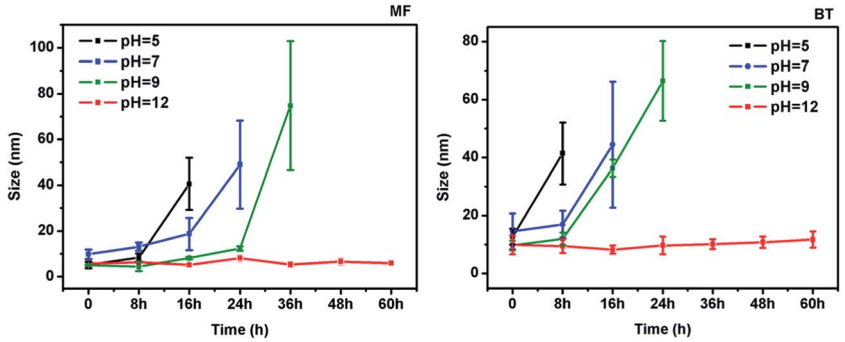

Fig. 10 Comparison of colloidal stability between MF–BSA–QDs synthesized in 5 min and BT–BSA–QDs synthesized in 4 hours at different pH values (5, 7, 9 and 12) for 60 hours.

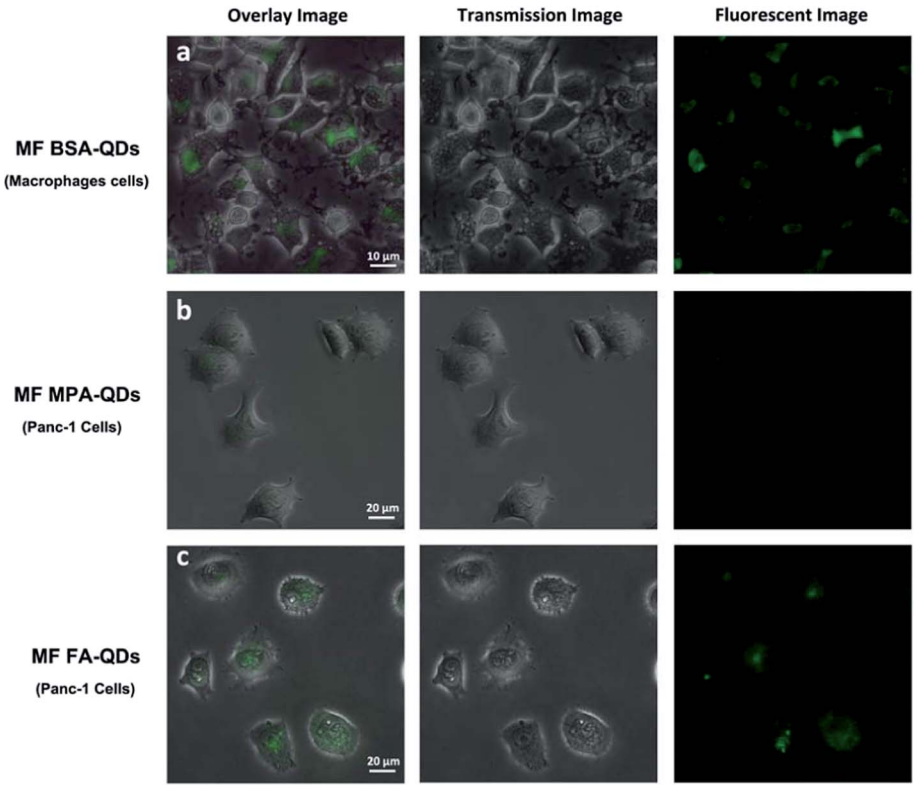

Fig. 11 Microscopic images of (a) RAW264.7 cells labeled with MF–BSA–QDs, (b) Panc-1 cells labeled with MF–MPA–QDs and (c) Panc-1 cells labeled with MF–FA–QDs.

3. Conclusions

In summary, we presented a detailed study on using microfluidic chips for the synthesis of BSA-conjugated CdTe QDs. We demonstrated that microfluidic chips are more convenient, time-saving and effective in preparing biofunctionalized QDs at mild temperatures compared to the conventional bench-top hot colloidal synthesis method. Systematic theoretical modeling was performed to investigate the impact of reaction temperature, and channel width and length of the microfluidic device on the kinetic growth rate of QDs. Thereafter, this simulated result was compared with the experimental work for further verification. Our experimental result showed good agreement with the simulation data. Both experimental and simulation results showed that reaction temperature, channel width and length of the microfluidic device play an important role in determining the flow velocity profile of the reaction agents and the final yield of QDs. Because biofunctionalized QDs can be used as optical probes for bioimaging, our work will certainly open up new avenues for developing highly integrated microfluidic systems that are capable of preparing biocompatible functionalized QDs for direct usage in cell and tumor imaging without the need of multiple rounds of washing, size selection and purification of QDs particles.

4. Methods

4.1. Materials

Cadmium perchlorate hydrate (99.999%), tellurium powder (99.8%), sodium borohydride (99.99%), 3-mercaptopropionic acid (MPA, ≥99%), albumin from bovine serum (BSA, ≥98%) and folic acid (FA, ≥97%) were purchased from Sigma-Aldrich. 10× Tris–acetate–EDTA (TAE, pH = 8.0) and agarose powder were purchased from Vivantis Ltd. Sodium hydroxide (NaOH, AR) and hydrochloric acid (HCl, AR) were purchased from Sinopharm Chemical Reagent Co., Ltd. All the chemicals were used as received without further purification. Deionized (DI) water, used in all the studies, was purified by a Milli-Q water purification system.

4.2. Design and fabrication of microfluidic chips

Microfluidic chips used for one-step biofunctionalized QD synthesis were fabricated through soft-lithography and replica-molding methods.[4,10] Briefly, negative photoresist SU-8 (GM1070, Gersteltec Engineering Solutions, Swiss) was spin coated onto a 4-inch silicon wafer (Semiconductor Wafer, Inc. Taiwan), followed by the UV patterning of the channels (3 min, lamp power: 355 W) to form a master. The wafer was then developed using an AZ developer (Branchburg, NJ) to remove the unexposed photoresist. PDMS mixture containing a curing agent and a base resin (Dow Corning, US) at a weight ratio of 1 : 10 was poured onto the master and cured at 120 °C for 10 min. The cured PDMS layer with microfluidic channels was then carefully peeled off from the master and stamped onto a glass slide.

4.3. Bench-top synthesis of MPA–CdTe QDs, BSA–CdTe QDs and FA–CdTe QDs

Te precursor was prepared by reducing 4 mg of tellurium powder with 10 mg of sodium borohydride ($NaBH_4$) in 1 mL nitrogen-saturated DI water at room temperature. The mixture was stirred for 1–2 hours until it turned colorless.

MPA–CdTe QDs were synthesized by our previous reported method in ref. 40 and 50. Briefly, 31 mg of cadmium perchlorate, 17 μL of MPA with concentrations ranging from 0 mM to 0.2 mM and 20 mL of nitrogen-saturated water were loaded into a three-necked flask with stirring. pH was adjusted to 9 by the dropwise addition of sodium hydroxide solution. The flask was sealed and then the Te precursor was injected into the mixture under a nitrogen atmosphere. The reaction mixture was slowly heated under a nitrogen atmosphere to 98 °C. After 2 min, 10 mL of mixture solution was collected as MPA–CdTe QDs nucleates for further microfluidic synthesis. We measured the UV-Vis and PL spectra of the MPA–CdTe QD nucleates. These spectra revealed a very weak feature of QDs. Such nucleates are very unstable and can be easily precipitated from water as time progresses.

To synthesize BSA–CdTe QDs, a BSA stock solution (100 mg mL^{-1}) was first prepared by dissolving protein powder (BSA) in 1× PBS. For the synthesis of QD, 2 mL of BSA (concentration: 0, 0.25, 0.5, 1.0, 2.0 or 5.0 mg mL^{-1}) was added together with 31 mg of cadmium perchlorate, 17 μL of MPA with concentrations ranging from 0 mM to 0.2 mM and 20 mL of nitrogen-saturated water into a three-necked flask under stirring at room temperature. The pH of the mixture was adjusted to 9 by dropwise titration with sodium hydroxide solution. After a quick injection of fresh Te precursor, the reaction mixture was vigorously stirred and heated to 65 °C under a nitrogen atmosphere. Within 2 min, 10 mL of mixture solution was collected as BSA–QD nucleates for further microfluidic synthesis. We measured the UV-Vis and PL spectra of the BSA–CdTe QD nucleates. These spectra revealed a very weak feature of QDs. Such nucleates are very unstable and can be easily precipitated from water as time progresses. The synthesis protocol of folic acid (FA)-functionalized CdTe is the same as BSA–CdTe QDs, except that the BSA stock solution was replaced by folic acid stock solution with concentrations of 0, 0.8, 1.6, 3.2, or 6.4 mg mL^{-1}.

4.4. Microfluidic synthesis of MPA–CdTe QDs, BSA–CdTe QDs and FA–CdTe QDs

Solutions containing MPA–CdTe QDs, BSA–CdTe QDs and FA–CdTe QDs nucleates were first obtained, as described in Section 4.3. A syringe pump was used to inject nucleate reagents into the inlet of the microfluidic chips at a constant flow rate of 500 μL min^{-1}. MPA–CdTe QDs, BSA–CdTe QDs and FA–CdTe QDs were formed as the reaction mixture flowed continuously through the microfluidic channel, which was heated from below using a hot plate at different temperatures of 98 °C, 150 °C, 180 °C, 200 °C, or 220 °C for different batches of MPA–CdTe QDs and 50 °C, 65 °C, 85 °C, or 100 °C for different batches of BSA–CdTe QDs and FA–CdTe QDs. During the optimization process for the channel width of the microfluidic chips (200 μm, 400 μm, 600 μm) in QDs syntheses, we maintained the channel length at 800 mm and the reaction temperature at an optimum value of 180 °C for MPA–CdTe QDs and 65 °C for BSA–CdTe QDs and FA–CdTe QDs.

4.5. Purification of QDs

QD samples were mixed with equal amounts of ethanol and then centrifuged at 10 000 rpm for 5 min to remove unreacted precursors and free ligand molecules. A centrifuge with a 100 kDa cut-off filter was used for purifying the BSA–CdTe QDs. 3 kDa cut-off filters were used to purify MPA–CdTe QDs and FA–CdTe QDs.

4.6. Optical characterization

The photoluminescence emission spectra of QDs were measured by a Fluorolog-3 Fluorometer (HORIBA Jobin Yvon, Edison, NJ USA) with an excitation wavelength of 400 nm. UV-Visible absorption spectra were collected using a spectrophotometer (Shimadzu UV-2450). Fourier transform infrared (FT-IR) spectra were obtained on a Shimadzu FT-IR spectrometer. In the FT-IR characterization, the QDs powder was mixed with potassium bromide (KBr) at 1 : 10 (w/w), ground, and compressed into tablets.

4.7. Simulation of QDs reaction in the microfluidic chips

To assess the performance of our designed microfluidic chips for the QDs reaction, we simulated the laminar flow inside the MF channel using finite element method (FEM) software (COMSOL Multiphysics 4.3a). Simulation studies were carried out by coupling the Navier–Stokes equation (eqn (3)), the continuity equation (eqn (4)) and the mass balance equation (eqn (5)).

$$-\nabla\cdot\mu(\nabla u + (\nabla u)^T) + \rho(u\cdot\nabla)u + \nabla p = F \quad (3)$$

$$\nabla\cdot u = 0 \quad (4)$$

$$\nabla\cdot(-D\nabla c + cu) = 0 \quad (5)$$

In the abovementioned equations, μ is the viscosity, u the velocity, ρ the density, p the pressure, F the sum of the body forces, D the diffusion coefficient, and c the concentration. These equations were solved for 3D geometry, as shown in Fig. 2. The diffusion coefficient (D) was set at $5 \times 10^{-7}e^{(-2000/T)}$. T is the temperature of the reaction (K). The fluid density (ρ) and fluid viscosity (μ) were set as the default values of water related to T. For the Navier–Stokes equation, a flow rate of 500 μL min^{-1} at the inlet was used. According to the boundary conditions, the velocity was zero at the channel walls. To solve the mass balance equation, a concentration of 10 mM of Cd^{2+} reactive species and 3.3 mM of Te^{2-} reactive species at the inlet were used.

4.8. Calculation of QDs particle number per liter

We first calculated the molar concentration of the CdTe nanocrystals using the Lambert–Beer's law.

$$C = \frac{A}{\varepsilon L} \quad (6)$$

In eqn (6), C is the molar concentration of the CdTe nanocrystals. A is the absorbance at the absorption peak of our CdTe sample solution. L is the path length of the radiation beam, which was fixed at 1 cm. ε is the extinction coefficient per mole of nanocrystals. In our calculation, ε value is based on eqn (7), an empirical function of the size of CdTe nanocrystals from Peng *et al.*[49] Here, we assumed the particle size to be 1.5 nm.

$$\varepsilon = 10043(D)^{2.12} \quad (7)$$

Then, we used eqn (8) to obtain the particle number of CdTe QDs per liter.

$$n_p = \frac{N}{V} = \frac{n}{V}N_A = \frac{CV}{V}N_A = CN_A \quad (8)$$

In eqn (8), n_p is the particle number of the CdTe nanocrystals per liter. V is the volume of the CdTe sample solution. N is the particle number of the CdTe nanocrystals. N_A is the Avogadro constant. n is the amount of CdTe nanocrystals. C is the molar concentration of the CdTe nanocrystals.

4.9. Photostability and colloidal stability measurements of QDs

For the photostability measurements, QDs samples were continuously excited by a G10T8 UV lamp (watts: 10 W, spectral output: 254 nm), and the photoluminescence emission spectra were recorded once every hour. For colloidal stability measurements, the QDs after purification were dispersed in solutions with different pH values (5, 7, 9, and 12). A 90Plus particle size analyzer (Brookhaven Instruments, NY USA) was used in this study. The photoluminescence emission spectra and DLS data were recorded once every 12 hours.

4.10. Agarose gel electrophoresis

The QD sample used for the agarose gel electrophoresis was a mixture of 10 μL of purified QD solution with 30 μL of sodium hydroxide solution (pH = 12). The running buffer was obtained by mixing 1% agarose gel with 1× TAE solution (Tris–acetate–EDTA). The QD sample was then loaded into the running buffer and electrophoresed at a constant voltage of 110 V for 15 min at room temperature.

4.11. Cellular uptake of MF–BSA–QDs and MF–FA–QDs

RAW264.7 macrophage cells and human pancreatic cancer cells, Panc-1 (CRL-1469, American Type Culture Collection) were cultured with Dulbecco's modified eagle's medium (DMEM, Hyclone) supplemented with 10% fetal bovine serum (FBS, Hyclone), penicillin (100 μg mL^{-1}, Gibco) and streptomycin (100 μg mL^{-1}, Gibco) in a humidified environment (37 °C, 5% CO_2). Before treating with QDs, the cells were seeded onto cover glasses in a 6-well plate with DMEM medium. The prepared QD formulations were then diluted with PBS buffer (pH = 7.2) solution to a concentration range of 10 to 20 μg mL^{-1}. Next, the cells were treated with QD formulations for 4 hours. After 4 hours of incubation, the treated cells were washed with PBS buffer three times. A Nikon Eclipse Ti inverted Microscope with 40× and 20× oil-immersion lens was used for the macrophage and Panc-1 cell imaging study. The cytotoxicity of the MF–BSA–QD formulations was also evaluated by the MTT assays (Fig. S3†).

References

1 G. M. Whitesides, *Nature*, 2006, **442**, 368–373.
2 A. J. deMello, *Nature*, 2006, **442**, 394–402.
3 K. S. Elvira, X. C. i. Solvas, R. C. R. Wootton and A. J. deMello, *Nat. Chem.*, 2013, **5**, 905–915.
4 P. Song, D. Jian, H. Tng, R. Hu, G. Lin, E. Meng and K.-T. Yong, *Adv. Healthcare Mater.*, 2013, **2**, 1170–1178.
5 J. Yan, M. Hu, D. Li, Y. He, R. Zhao, X. Jiang, S. Song, L. Wang and C. Fan, *Nano Res.*, 2008, **1**, 490–496.
6 A. D. Stroock, S. K. W. Dertinger, A. Ajdari, I. Mezić, H. A. Stone and G. M. Whitesides, *Science*, 2002, **295**, 647–651.
7 K. S. Krishna, Y. Li, S. Li and C. S. S. R. Kumar, *Adv. Drug Delivery Rev.*, 2013, **65**, 1470–1495.
8 S. Yao, Y. Shu, Y.-J. Yang, X. Yu, D.-W. Pang and Z.-L. Zhang, *Chem. Commun.*, 2013, **49**, 7114–7116.
9 V. Vickerman, J. Blundo, S. Chung and R. Kamm, *Lab Chip*, 2008, **8**, 1468–1477.

10 T. Danny Jian Hang, P. Song, R. Hu, C. Yang and K.-T. Yong, *Analyst*, 2014, **139**, 407–415.
11 D. J. H. Tng, R. Hu, P. Song, I. Roy and K.-T. Yong, *Micromachines*, 2012, **3**, 615–631.
12 P. Song, R. Hu, D. J. H. Tng and K.-T. Yong, *RSC Adv.*, 2014, **4**, 11499–11511.
13 J. B. Edel, R. Fortt, J. C. deMello and A. J. deMello, *Chem. Commun.*, 2002, 1136–1137.
14 J. Huang, L. Lin, Q. Li, D. Sun, Y. Wang, Y. Lu, N. He, K. Yang, X. Yang, H. Wang, W. Wang and W. Lin, *Ind. Eng. Chem. Res.*, 2008, **47**, 6081–6090.
15 X. Z. Lin, A. D. Terepka and H. Yang, *Nano Lett.*, 2004, **4**, 2227–2232.
16 S. E. Lohse, J. R. Eller, S. T. Sivapalan, M. R. Plews and C. J. Murphy, *ACS Nano*, 2013, **7**, 4135–4150.
17 J. Wagner and J. M. Kohler, *Nano Lett.*, 2005, **5**, 685–691.
18 Y. Song, L. L. Henry and W. Yang, *Langmuir*, 2009, **25**, 10209–10217.
19 Y. Song, H. Modrow, L. L. Henry, C. K. Saw, E. E. Doomes, V. Palshin, J. Hormes and C. S. S. R. Kumar, *Chem. Mater.*, 2006, **18**, 2817–2827.
20 T. H. Eun, S.-H. Kim, W.-J. Jeong, S.-J. Jeon, S.-H. Kim and S.-M. Yang, *Chem. Mater.*, 2009, **21**, 201–203.
21 M. Takagi, T. Maki, M. Miyahara and K. Mae, *Chem. Eng. J.*, 2004, **101**, 269–276.
22 H. Wang, H. Nakamura, M. Uehara, M. Miyazaki and H. Maeda, *Chem. Commun.*, 2002, 1462–1463.
23 L. Frenz, A. El Harrak, M. Pauly, S. Bégin-Colin, A. D. Griffiths and J.-C. Baret, *Angew. Chem., Int. Ed.*, 2008, **47**, 6817–6820.
24 S. A. Khan, A. Günther, M. A. Schmidt and K. F. Jensen, *Langmuir*, 2004, **20**, 8604–8611.
25 E. M. Chan, A. P. Alivisatos and R. A. Mathies, *J. Am. Chem. Soc.*, 2005, **127**, 13854–13861.
26 E. M. Chan, R. A. Mathies and A. P. Alivisatos, *Nano Lett.*, 2003, **3**, 199–201.
27 M. Mirhosseini Moghaddam, M. Baghbanzadeh, A. Sadeghpour, O. Glatter and C. O. Kappe, *Chem.–Eur. J.*, 2013, **19**, 11629–11636.
28 B. H. Kwon, H. Kim, Y. Kim, D. Kang and D. Young Jeon, *Electrochem. Solid-State Lett.*, 2013, **2**, R27–R30.
29 A. M. Nightingale and J. C. de Mello, *ChemPhysChem*, 2009, **10**, 2612–2614.
30 H. Wang, X. Li, M. Uehara, Y. Yamaguchi, H. Nakamura, M. Miyazaki, H. Shimizu and H. Maeda, *Chem. Commun.*, 2004, 48–49.
31 A. Abou-Hassan, R. Bazzi and V. Cabuil, *Angew. Chem., Int. Ed.*, 2009, **48**, 7180–7183.
32 B.-H. Kwon, K. G. Lee, T. J. Park, H. Kim, T. J. Lee, S. J. Lee and D. Y. Jeon, *Small*, 2012, **8**, 3257–3262.
33 M. Uehara, H. Nakamura and H. Maeda, in *World Congress on Medical Physics and Biomedical Engineering 2006*, ed. R. Magjarevic and J. H. Nagel, Springer, Berlin, Heidelberg, 2007, vol. 14, pp. 250–253.
34 A. M. Nightingale and J. C. de Mello, *J. Mater. Chem.*, 2010, **20**, 8454–8463.
35 P. M. Valencia, O. C. Farokhzad, R. Karnik and R. Langer, *Nat. Nanotechnol.*, 2012, **7**, 623–629.
36 X. G. Peng, *Nano Res.*, 2009, **2**, 425–447.
37 P. N. Prasad, *Nanophotonics*, John Wiley & Sons, Hoboken, 2004.
38 P. N. Prasad, *Introduction to nanomedicine and nanobioengineering*, Wiley, Hoboken, N.J., 2013.
39 X. Wang, W. W. Yu, J. Zhang, J. Aldana, X. Peng and M. Xiao, *Phys. Rev. B: Condens. Matter Mater. Phys.*, 2003, **68**, 125318.
40 Y. Wang, R. Hu, G. Lin, W.-C. Law and K.-T. Yong, *RSC Adv.*, 2013, **3**, 8899–8908.
41 S. Rauf, A. Glidle and J. M. Cooper, *Chem. Commun.*, 2010, **46**, 2814–2816.
42 J. K. Jaiswal and S. M. Simon, *Trends Cell Biol.*, 2004, **14**, 497–504.
43 C. X. Guo, H. B. Yang, Z. M. Sheng, Z. S. Lu, Q. L. Song and C. M. Li, *Angew. Chem., Int. Ed.*, 2010, **49**, 3014–3017.
44 C. X. Guo, J. Xie, B. Wang, X. Zheng, H. B. Yang and C. M. Li, *Sci. Rep.*, 2013, **3**, 2957.
45 C. X. Guo, D. Zhao, Q. Zhao, P. Wang and X. Lu, *Chem. Commun.*, 2014, **50**, 7318–7321.
46 S. Zeng, D. Baillargeat, H.-P. Ho and K.-T. Yong, *Chem. Soc. Rev.*, 2014, **43**, 3426–3452.
47 T. Zhao, X. Hou, Y.-N. Xie, L. Wu and P. Wu, *Analyst*, 2013, **138**, 6589–6594.
48 Y. Nakane, A. Sasaki, M. Kinjo and T. Jin, *Anal. Methods*, 2012, **4**, 1903–1905.
49 W. W. Yu, L. H. Qu, W. Z. Guo and X. G. Peng, *Chem. Mater.*, 2003, **15**, 2854–2860.
50 W.-C. Law, K.-T. Yong, I. Roy, H. Ding, R. Hu, W. Zhao and P. N. Prasad, *Small*, 2009, **5**, 1302–1310.
51 B. J. Kirby, *Micro- and Nanoscale Fluid Mechanics: Transport in Microfluidic Devices*, Cambridge University Press, New York, 2010.
52 A. Barth, *Biochim. Biophys. Acta, Bioenerg.*, 2007, **1767**, 1073–1101.
53 S. Hinds, B. J. Taft, L. Levina, V. Sukhovatkin, C. J. Dooley, M. D. Roy, D. D. MacNeil, E. H. Sargent and S. O. Kelley, *J. Am. Chem. Soc.*, 2006, **128**, 64–65.
54 B. A. Kairdolf, A. M. Smith and S. Nie, *J. Am. Chem. Soc.*, 2008, **130**, 12866–12867.
55 L. Ye, K. T. Yong, L. W. Liu, I. Roy, R. Hu, J. Zhu, H. X. Cai, W. C. Law, J. W. Liu, K. Wang, J. Liu, Y. Q. Liu, Y. Z. Hu, X. H. Zhang, M. T. Swihart and P. N. Prasad, *Nat. Nanotechnol.*, 2012, **7**, 453–458.
56 B. Zhang, R. Hu, Y. Wang, C. Yang, X. Liu and K.-T. Yong, *RSC Adv.*, 2014, **4**, 13805–13816.

